Title	Subsynchronous resonance damping control of thyristor-controlled series capacitor
Author(s)	Kakimoto, N; Phongphanphanee, A
Citation	IEEE TRANSACTIONS ON POWER DELIVERY (2003), 18(3): 1051-1059
Issue Date	2003-07
URL	http://hdl.handle.net/2433/50072
Right	(c)2003 IEEE. Personal use of this material is permitted. However, permission to reprint/republish this material for advertising or promotional purposes or for creating new collective works for resale or redistribution to servers or lists, or to reuse any copyrighted component of this work in other works must be obtained from the IEEE.
Type	Journal Article
Textversion	publisher; none

Subsynchronous Resonance Damping Control of Thyristor-Controlled Series Capacitor

Naoto Kakimoto, *Member, IEEE,* and Anan Phongphanphanee

***Abstract*—A thyristor-controlled series capacitor (TCSC) substantially improves transmission capacity. It also mitigates subsynchronous resonance (SSR) accompanying conventional series capacitors. With an appropriate angle of thyristor firing, electrical damping becomes almost zero, which is called SSR neutral. This quality comes from TCSC itself. However, negative damping still remains, and is large for firing angle $170\sim180^\circ$ where little current flows through thyristors. This paper deals with control of firing angle. First, we oscillate the firing angle at a given frequency, and present an analytical method of calculating electrical damping. Next, we show that the damping improves at all frequencies if the firing angle oscillation is in phase with that of rotor angle. Synchronizing torque decreases, however, so a limit must be put on the control gain. Lastly, we execute numerical simulations to verify our analytical results.**

***Index Terms*—Damping control, SSR, TCSC.**

I. Introduction

A THYRISTOR-CONTROLLED series capacitor (TCSC) compensates transmission line reactance, and increases or controls power transfer. It is also effective in mitigating subsynchronous resonance (SSR) [1]. It was shown with an analog simulator that electrical damping of a system with a TCSC is almost the same as one with no series compensation, that is, the TCSC is SSR neutral [2]. This is one of the most important attributes of the TCSC.

Several theoretical analyses and field tests of the TCSC were made in relation to SSR. It was shown with EMTP that a TCSC in vernier mode behaves as a lossy capacitor [3]. Field tests at the Slatt substation demonstrated that the TCSC does not participate in SSR [4]. Some dynamic models were derived based on Poincare mapping and others [5]–[8]. These models are useful in eigenvalue analyses of SSR. With Fourier analysis, some algebraic equations were derived for voltage and current components of a TCSC [9], [10]. By solving one algebraic equation, it is possible to calculate electrical damping of a system compensated with a TCSC [11].

If the conduction angle of thyristors is appropriately wide, the electrical damping is nearly equal to zero. The TCSC is therefore almost SSR neutral. If a generator has moderate damping, SSR does not occur. However, in a case where the firing angle is close to 180°, and the conduction angle is narrow, action of the TCSC is close to that of a series capacitor. It accordingly shows large negative damping. In order to operate in such cases, or in a case where damping of a generator is insufficient, the firing angle of the TCSC must be modulated [1]. In the field test of [4], to excite a torsional oscillation mode, rotor speed signals were used to modulate the firing angle of TCSC. It is hence clear that the modulation of the firing angle has some influence on SSR. The firing angle was fixed constant, however, in the preceding studies.

In this paper, we present a method of analytically calculating electrical damping of TCSC with a firing control. It is an expansion of techniques proposed in [10] and [11]. Rotor angle oscillation is used as an input signal. It is transmitted to the firing angle through a gain and a phase. We examine their influence. It seems natural to use deviation of rotor speed instead of angle. The phase is 90° in this case. However, it becomes clear that electrical damping improves in one frequency range, but it deteriorates in another range at the same time. On the other hand, if the phase is 0°, the firing angle oscillates in phase with the rotor angle. Now, the damping improves in all frequency range. It is also possible to turn the damping to positive. The synchronizing torque deteriorates, however, so some limit must be put on the gain.

First, we briefly describe a TCSC and a transmission system in Section II. We observe current components of a thyristor-controlled reactor (TCR) brought by firing angle oscillation, and derive analytical equations for them in Sections III and IV. In Sections V and VI, we present an algebraic equation for the TCSC and solve it to obtain electrical damping and to examine the effect the control has on damping. Lastly, we execute numerical simulations to verify our analytical results in Section VII.

II. Basic Equations

A. Transmission System With TCSC

Fig. 1 shows a transmission system compensated with a TCSC. Transmission line resistance r_o is 0.02 p.u., and reactance is $\omega_o L_o = 0.9$ p.u., where $\omega_o = 120\pi$. The base of per-unit system is 500 kV and 1000 MVA. The transmission line reactance is large, so it is compensated with TCSC. The capacitor is $1/\omega_o C = 0.3$ p.u., and the reactor is $\omega_o L = 0.0512$ p.u. The reactor has a resistance r of 0.002 p.u. The compensation is adjusted with the thyristors.

Time variations of transmission line current i, capacitor voltage v, and thyristor-controlled reactor (TCR) current i_l are described by the following equations:

$$\frac{di}{dt} = \frac{e - v_b - v - r_o i}{L_o} \tag{1}$$

$$\frac{dv}{dt} = \frac{i - i_l}{C} \tag{2}$$

$$\frac{di_l}{dt} = \begin{cases} (v - r i_l)/L & \text{(thyristor on)} \\ 0 & \text{(thyristor off)} \end{cases} \tag{3}$$

Manuscript received September 12, 2001; revised April 18, 2002.
N. Kakimoto is with Kyoto University, Kyoto 606-8501, Japan.
A. Phongphanphanee is with Fujikura Ltd., Chiba 285-8550, Japan.
Digital Object Identifier 10.1109/TPWRD.2003.813627

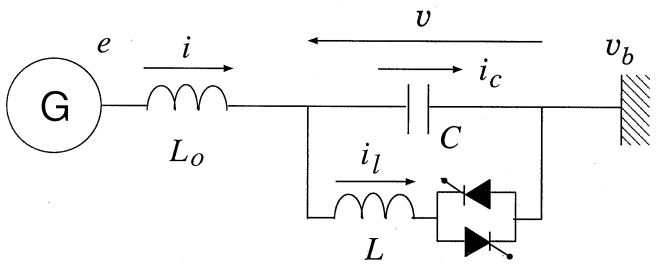

Fig. 1. Transmission system with TCSC.

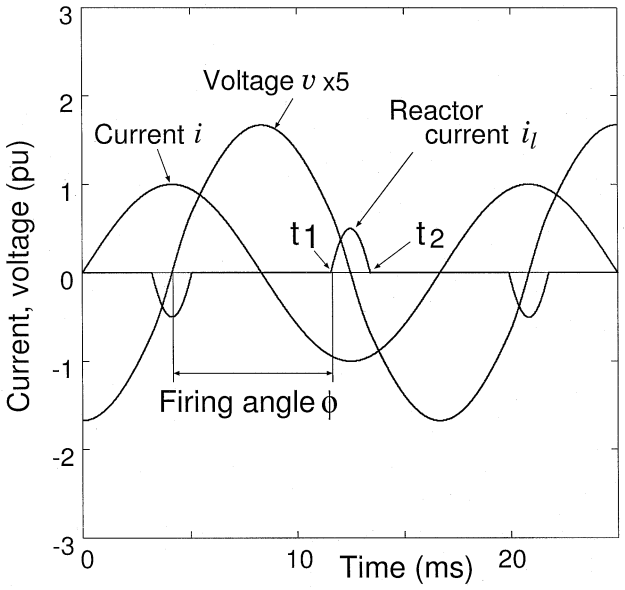

Fig. 2. Voltage and current of TCSC.

where e is the internal voltage of the generator. Its amplitude is 1 p.u. The subtransient reactance is included in the transmission line reactance. v_b is the infinite bus voltage (1 p.u.). Fig. 2 shows time variations of the voltage v and the reactor current i_l for a case where TCSC is driven by the current i with amplitude 1 p.u., and frequency 60 Hz. The thyristors are triggered at firing angle ϕ from zero-crossing points of the voltage v.

The reactor current i_l contains some odd harmonics besides a fundamental wave. The voltage v is multiplied by 5 for the sake of comparison. Small odd harmonics are superimposed on a fundamental wave, as observed from the figure.

B. Generator-Turbine Shaft System

Fig. 3 shows a model of the generator-turbine shaft system [12]. It consists of six masses. The motion of each mass is described by the following equations:

$$m_1 \frac{d^2\delta_1}{dt^2} = p_{m1} - k_{12}\delta_{12} - d_1\omega_1 \tag{4}$$

$$m_2 \frac{d^2\delta_2}{dt^2} = p_{m2} - k_{12}\delta_{21} - k_{23}\delta_{23} - d_2\omega_2 \tag{5}$$

$$m_3 \frac{d^2\delta_3}{dt^2} = p_{m3} - k_{23}\delta_{32} - k_{34}\delta_{34} - d_3\omega_3 \tag{6}$$

$$m_4 \frac{d^2\delta_4}{dt^2} = p_{m4} - k_{34}\delta_{43} - k_{45}\delta_{45} - d_4\omega_4 \tag{7}$$

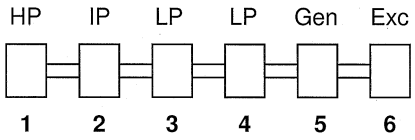

Fig. 3. Generator-turbine shaft system.

TABLE I
PARAMETERS OF GENERATOR-TURBINE SHAFT (per unit)

H_i	D_i	k_{ij}
H_1=0.0929	D_1=0.012	k_{12}=19.303
H_2=0.1556	D_2=0.001	k_{23}=34.929
H_3=0.8587	D_3=0.085	k_{34}=52.038
H_4=0.8842	D_4=0.080	k_{45}=70.858
H_5=0.8685	D_5=0.200	k_{56}=2.8220
H_6=0.0342	D_6=0.018	

TABLE II
EIGENVALUES OF GENERATOR-TURBINE SHAFT

Mode	Eigenvalue
1	-0.011±j47.456
2	-0.031±j32.285
3	-0.031±j25.547
4	-0.120±j20.211
5	-0.043±j15.712
6	-0.068±j 0.000

(The imaginary part is in Hz)

$$m_5 \frac{d^2\delta_5}{dt^2} = -p_e - k_{45}\delta_{54} - k_{56}\delta_{56} - d_5\omega_5 \tag{8}$$

$$m_6 \frac{d^2\delta_6}{dt^2} = -k_{56}\delta_{65} - d_6\omega_6 \tag{9}$$

where for each mass i, m_i is inertia constant, δ_i is rotor angle, p_{mi} is mechanical power input, k_{ij} is torsional spring constant between mass i, and j, d_i is damping torque coefficient, $\delta_{ij} \equiv \delta_i - \delta_j$, $\omega_i = d\delta_i/dt$, is rotor speed, p_e is electrical power output. The rotor angle δ_5 in (8) corresponds to the phase δ of the internal voltage e. Table I shows constants of the shaft system, where $m_i = H_i/60\pi$, $d_i = D_i/120\pi$. The fraction of the total mechanical power effected by each of the masses p_{m1} to p_{m4} is 20, 20, 30, 30%, respectively.

There are six natural modes in the shaft system of Fig. 3. Table II shows eigenvalues for the modes. The modes 1∼5 correspond with torsional oscillation modes. The mode 6 is a rigid body mode in which all masses move together. This mode becomes a swing mode when the generator is connected to the transmission system.

III. CONTROL OF FIRING ANGLE

Assume the rotor angle of the generator oscillates at a frequency f, then two voltage components appear besides a fundamental component. Their frequencies are $\hat{f} = f_o \pm f$, where $f_o = 60$ Hz. Due to these voltage components, current components of frequency $\overline{f} = mf_o \pm \hat{f}$ appear in the TCR current, where m is an even number. Substituting $\hat{f}$ into this equation gives

$$\overline{f} = (m \pm 1)f_o \pm f \equiv nf_o \pm f. \tag{10}$$

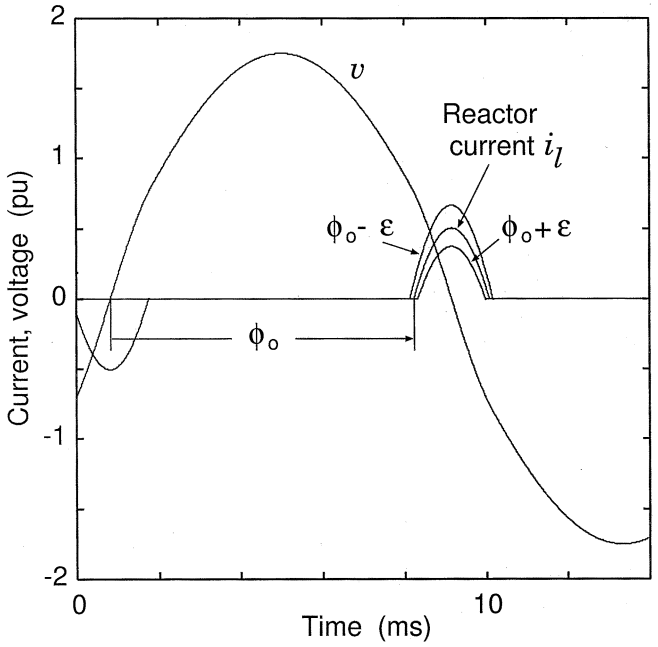

Fig. 4. Firing angle control.

The n is clearly an odd number. For example, if $f = 20$ Hz, $\overline{f}$ becomes $40, 80, 160, 200, 280, \ldots$. The most important components are 40 and 80 Hz.

Fig. 4 shows variation of the reactor current for changes of the firing angle. If the firing angle changes from ϕ_o to $\phi_o - \varepsilon$, then the reactor current increases. Conversely, if it changes to $\phi + \varepsilon$, the current decreases. In this paper, to suppress SSR, we oscillate the firing angle at the same frequency f as the rotor angle

$$\phi = \phi_o + \varepsilon \sin(2\pi f t + \theta) = \phi_o + \Delta\phi \tag{11}$$

where ε and θ are, respectively, the amplitude and phase of the oscillation.

The TCSC voltage v contains odd harmonics, and is expressed as follows:

$$v(t) = \sum a_i \sin 2\pi i f_o t \tag{12}$$

where a_i is an amplitude, and i is an odd number. Fig. 5 shows variations of the TCR current due to the oscillation of the firing angle, where the voltage is assumed to contain only fundamental component, and $a_1 = 1$ p.u. The parameters of the firing angle are $\phi_o = 160°$, $\varepsilon = 1°$, $f = 20$ Hz, $\theta = 0$. From the figure, it is seen that the current components have frequencies 40, 80, 160, 200, 280, ... Hz. These frequencies are represented by $nf_o \pm f$ Hz, where n is odd number. These frequencies prove to be the same as those produced by oscillating the rotor angle at f Hz, as shown in (10).

IV. Analytical Equation

In this section, we derive analytical equations for the variation of the TCR current caused by the firing angle oscillation. First, from (3) and (12), the reactor current i_l is given by

$$i_l = \sum \frac{a_i}{i\omega_o L} (\cos i\omega_o t_1 - \cos i\omega_o t). \tag{13}$$

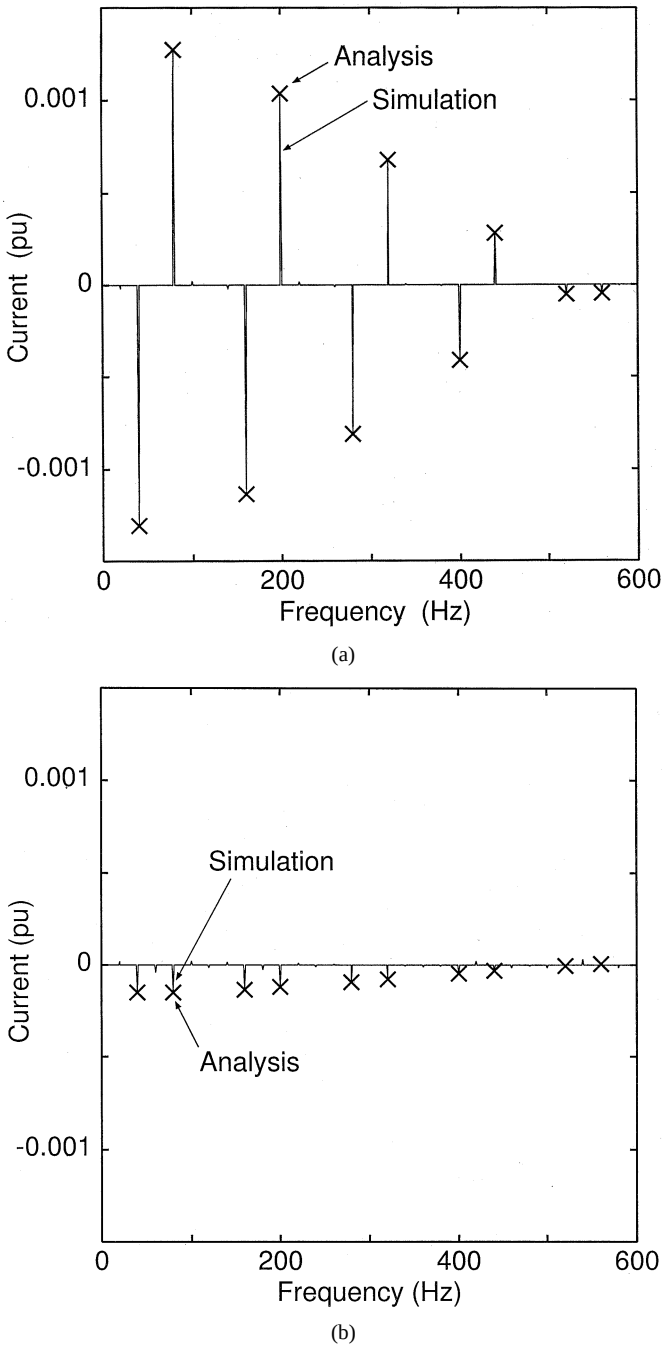

Fig. 5. Variation of TCR current. (a) In-phase components. (b) Quadrature components.

For simplicity, we assumed $r = 0$. The t_1 is a time when the current begins to flow, and $\omega_o = 2\pi f_o$. The components of frequency $(nf_o + f)$ Hz are obtained by

$$i_{ls} = \frac{2}{T} \int_0^T i_l \sin(n\omega_o + \omega)t \, dt \tag{14}$$

$$i_{lc} = \frac{2}{T} \int_0^T i_l \cos(n\omega_o + \omega)t \, dt. \tag{15}$$

T is an interval of the integration, and $\omega = 2\pi f$. The integrals in (14) and (15) are obtained by calculating for each current pulse

$(k = 0, 1, 2, \ldots)$, and then by summing all of them. Hence we first calculate

$$i_{lsk} \equiv \int_{t_1}^{t_2} i_l \sin(n\omega_o + \omega)t\, dt \tag{16}$$

$$i_{lck} \equiv \int_{t_1}^{t_2} i_l \cos(n\omega_o + \omega)t\, dt \tag{17}$$

where the t_2 is the time when the current stops flowing.

A. Variations in Times t_1 and t_2

Set as $\theta = 0$ in (11), then

$$\phi = \phi_o + \varepsilon \sin \omega t. \tag{18}$$

The time t_1 when the current begins to flow satisfies

$$\omega_o t_1 = k\pi + \phi \tag{19}$$

where $k = 0, 1, 2, \ldots$. Let $t_1 = t_1^o + \Delta t_1$ (where the superscript "o" denotes the steady-state value for $\varepsilon = 0$), then

$$\Delta t_1 \approx \frac{\varepsilon}{\omega_o} \sin h(k\pi + \phi_o) \tag{20}$$

is obtained, where

$$h \equiv \omega/\omega_o.$$

The time t_2 varies due to Δt_1, and we set as $t_2 = t_2^o + \Delta t_2$.

B. In-Phase Components

Substitute $t_1 = t_1^o + \Delta t_1$ and $t_2 = t_2^o + \Delta t_2$ into (16), and arrange it up to the first order of ε, then

$$i_{lsk} \simeq i_{lsk}^o + \varepsilon \sum a_i \frac{\sin i\phi \cos h\overline{\phi} \sin(n+h)\overline{\phi}}{\omega_o^2 L(n+h)} \tag{21}$$

is obtained, where i_{lsk}^o is a constant, and

$$\overline{\phi} \equiv \pi - \phi.$$

For the derivation of (21), refer to the Appendix. The current component i_{ls} in (14) is obtained by summing the i_{lsk} for all k. Its variation is given by

$$\Delta i_{ls} = \varepsilon a \tag{22}$$

where

$$a = \frac{2\alpha}{\omega_o L\pi(n+h)} \cos h\overline{\phi} \sin(n+h)\overline{\phi}$$

$$\alpha = \sum a_i \sin i\phi.$$

C. Quadrature Components

Substitute $t_1 = t_1^o + \Delta t_1$ and $t_2 = t_2^o + \Delta t_2$ into (17), and arrange it again, then

$$\Delta i_{lc} = \varepsilon b \tag{23}$$

is obtained, where

$$b = -\frac{2\alpha}{\omega_o L\pi(n+h)} \sin h\overline{\phi} \sin(n+h)\overline{\phi}.$$

Equations (22) and (23) represent the variation of the TCR current for the oscillation of the firing angle. Fig. 5 shows analytical values obtained by the above equations. The values agree very well with the simulation results.

D. Generalization

Next, we set $\theta = \pi/2$ in (11), then ϕ changes as

$$\phi = \phi_o + \varepsilon \cos \omega t. \tag{24}$$

In this case, the current components are given by

$$\Delta i_{ls} = \varepsilon c, \qquad \Delta i_{lc} = \varepsilon d \tag{25}$$

where

$$c = -b, \qquad d = a.$$

The components of frequency $(nf_o - f)$ Hz, as is clear from the definition in (14) and (15), are given by replacing as follows:

$$n \to -n, \qquad a \to -a, \qquad c \to -c \tag{26}$$

in (22), (23), and (25).

In a general case where the firing changes according to (11), ϕ varies as

$$\phi = \phi_o + \varepsilon \cos\theta \sin \omega t + \varepsilon \sin\theta \cos \omega t.$$

In this case, the current components are given by

$$\Delta i_l \equiv \begin{pmatrix} \Delta i_{ls} \\ \Delta i_{lc} \end{pmatrix} = \varepsilon p \tag{27}$$

where p is a vector

$$p = \begin{pmatrix} a & c \\ b & d \end{pmatrix} \begin{pmatrix} \cos\theta \\ \sin\theta \end{pmatrix}.$$

V. Network Equation

A. Representation of TCSC

As observed in Sections III and IV, if the firing angle oscillates at a frequency f, small current components of frequencies $f_i = nf_o \pm f$ (n: odd number) flow through the TCR. If $f = 20$ Hz, then $f_i = 40, 80, 160, 200, 280$ Hz, $\ldots$ $(i = 1, 2, 3, \ldots)$. These components flow through the capacitor and the transmission line, and corresponding voltage components appear on the TCSC. Now let $\Delta i_1, \Delta i_2, \Delta i_3, \ldots, \Delta v_1, \Delta v_2, \Delta v_3, \ldots$ denote these small current and voltage components from low to high frequencies in sequence,

where

$$\Delta i_i = \begin{pmatrix} \Delta i_{si} \\ \Delta i_{ci} \end{pmatrix}, \qquad \Delta v_i = \begin{pmatrix} \Delta v_{si} \\ \Delta v_{ci} \end{pmatrix}.$$

The subscript "s, c" mean $\sin$ and $\cos$ components, respectively. These current and voltage components are related as follows [10]:

$$\Delta I = Y \Delta V + \varepsilon P \tag{28}$$

where $\Delta I = (\Delta i_1^t, \Delta i_2^t, \ldots)^t$, $\Delta V = (\Delta v_1^t, \Delta v_2^t, \ldots)^t$. Y is an admittance matrix

$$Y = Y_l + Y_c.$$

Y changes with method of firing thyristors. In this paper, we choose zero-crossing points of the fundamental voltage as the reference of firing. Y_l is an admittance matrix of the TCR. It is composed of 2×2 matrices y_{lij}

$$y_{lij} = \begin{pmatrix} \pm g_{ij} & \mp b_{ij} \\ b_{ij} & g_{ij} \end{pmatrix}$$

where for $i, j = 1, 2, 3, \ldots$

$$g_{ij} = \frac{2}{\omega_o L \pi h_j} \frac{\sin h_i\overline{\phi} \sin h_j\overline{\phi}}{h_i}$$

$$b_{ij} = \frac{2}{\omega_o L \pi h_j} \left(\frac{\sin h_i\overline{\phi} \cos h_j\overline{\phi}}{h_i} - \frac{\sin m\overline{\phi}}{m} \right).$$

h_i, h_j, m (even number) are related as follows:

$$h_i = f_i/f_o = m \pm h_j, \qquad h_j = f_j/f_o.$$

Y_c is an admittance matrix of the capacitor

$$Y_c = diag\{y_{c1}, y_{c2}, \ldots\} \tag{29}$$

where y_{ci} $(i = 1, 2, 3, \ldots)$ is a 2×2 matrix

$$y_{ci} = \begin{pmatrix} 0 & -2\pi f_i C \\ 2\pi f_i C & 0 \end{pmatrix}.$$

P is a vector which represents small current components caused by the oscillation of the firing angle

$$P = (p_1^t, p_2^t, \ldots)^t. \tag{30}$$

p_i denotes a vector p of (27) corresponding to the frequency f_i, where $f_i/f_o = n \pm h$.

B. Installation Into Transmission System

If the rotor of the generator oscillates at a frequency f, then two voltage components of frequencies $f_o \pm f$ appear. Let a vector ΔE denote these components

$$\Delta E = (\Delta e_1, \Delta e_2, \ldots)^t.$$

e_i corresponds with v_i, i_i. In a range $0 < f < 60$ Hz, only Δe_1 and Δe_2 are nonzero, and other Δe_is are zero. On the other hand, the infinite bus voltage does not change. Hence, ΔV and ΔI of the TCSC are related as follows:

$$\Delta E - \Delta V = Z_o \Delta I. \tag{31}$$

Z_o is an impedance matrix of the transmission line

$$Z_o = diag\{z_{o1}, z_{o2}, \ldots\}$$

where z_{oi} is a 2×2 matrix

$$z_{oi} = \begin{pmatrix} r_o & -2\pi f_i L_o \\ 2\pi f_i L_o & r_o \end{pmatrix}.$$

From (28) and (31), we obtain

$$(1 + Y Z_o)\Delta I = Y \Delta E + \varepsilon P. \tag{32}$$

VI. Damping Torque

A. Definition of Torque

Interaction between the shaft system and the transmission system occurs through the generator output $p_e = ei$. Now, let the rotor angle of the generator oscillate at a frequency f around an operating point δ_o as follows:

$$\delta = \delta_o + \varepsilon' \sin \omega t = \delta_o + \Delta\delta \tag{33}$$

where ε' is an amplitude, and $\omega = 2\pi f$. Numerically integrate (1)$\sim$(3) to obtain time variation of p_e, and extract a component of frequency f with the fast Fourier transformation (FFT), then p_e is expressed as follows:

$$p_e \simeq p_{eo} + \varepsilon' k_e \sin \omega t + \varepsilon' d_e \omega \cos \omega t. \tag{34}$$

The first term is a steady state value, the second term is a synchronizing torque, and the third term is a damping torque. k_e and d_e represent a synchronizing and a damping torque coefficient, respectively.

B. Analytical Equations for k_e and d_e

Set the generator and the infinite bus voltages e, v_b as follows:

$$e = e_o \sin(\omega_o t + \delta), \qquad v_b = v_{bo} \sin(\omega_o t)$$

where e_o and v_{bo} are their amplitudes. Substitute (33) into the above equation, then e is transformed as

$$e \simeq e_o \sin(\omega_o t + \delta_o) - \frac{\varepsilon' e_o}{2} \sin\{(\omega_o - \omega)t + \delta_o\} + \frac{\varepsilon' e_o}{2} \sin\{(\omega_o + \omega)t + \delta_o\}. \tag{35}$$

The two components Δe_1, Δe_2 of Section V-B thus appear. Due to these voltages and the firing angle oscillations, the current i changes as follows:

$$i \simeq i_o \sin(\omega_o t + \delta_o + \psi_o) + \varepsilon' i_1 \sin\{(\omega_o - \omega)t + \delta_o + \psi_1\} + \varepsilon' i_2 \sin\{(\omega_o + \omega)t + \delta_o + \psi_2\} \tag{36}$$

where i_o, i_1, i_2 and ψ_o, ψ_1, ψ_2 are amplitudes and phases, respectively. i_1, i_2, ψ_1, ψ_2 are determined by solving (32). From (35) and (36), we obtain

$$\begin{aligned} p_e \simeq{}& \tfrac{1}{2} e_o i_o \cos\psi_o \\ &+ \varepsilon' \tfrac{1}{2} e_o (i_o \sin\psi_o + i_1 \sin\psi_1 - i_2 \sin\psi_2) \sin\omega t \\ &+ \varepsilon' \tfrac{1}{2} e_o (i_1 \cos\psi_1 + i_2 \cos\psi_2) \cos\omega t. \end{aligned}$$

Comparison with (34) gives

$$\begin{aligned} k_e &= \tfrac{1}{2} e_o (i_o \sin\psi_o + i_1 \sin\psi_1 - i_2 \sin\psi_2) \\ d_e &= \frac{1}{2\omega} e_o (i_1 \cos\psi_1 + i_2 \cos\psi_2). \end{aligned} \tag{37}$$

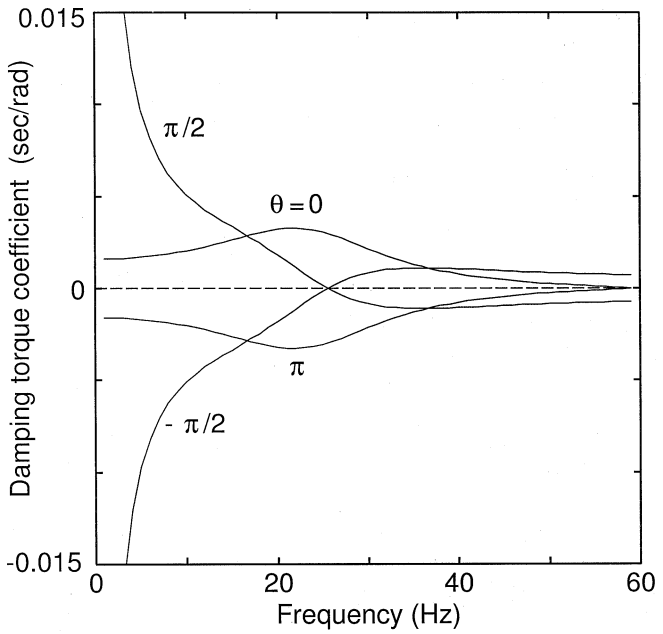

Fig. 6. Selection of phase θ.

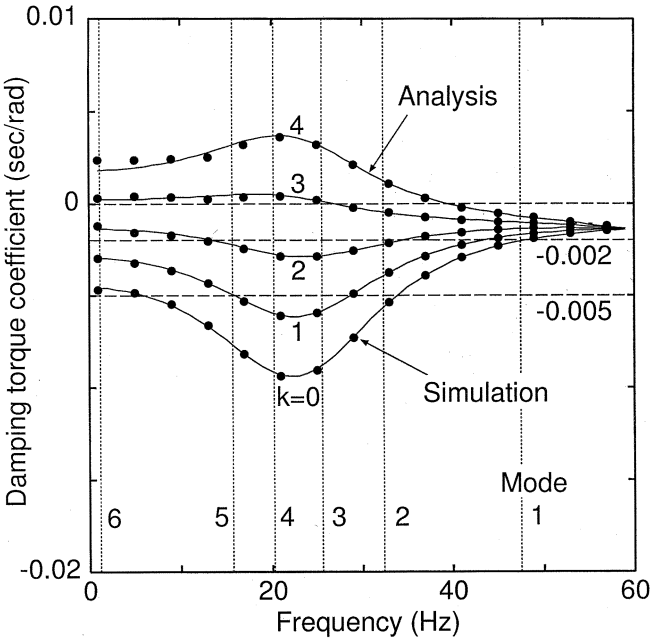

(a)

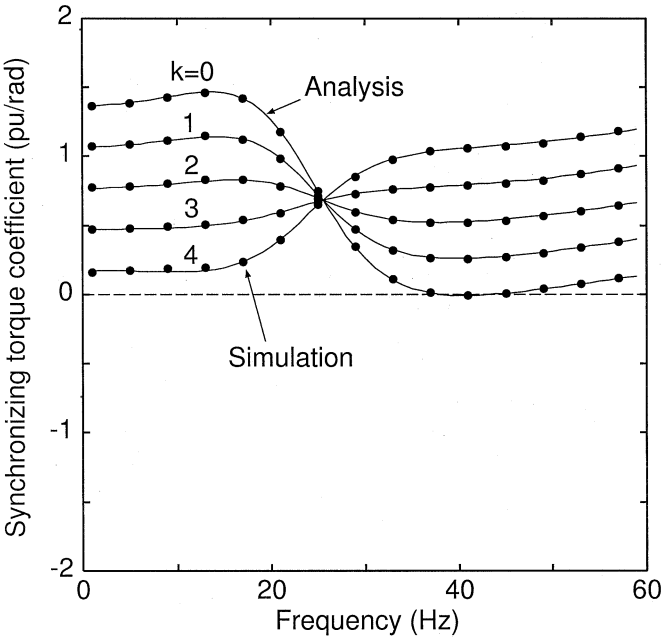

(b)

Fig. 7. Limitation of gain k. (a) Damping torque coefficient. (b) Synchronizing torque coefficient.

C. Damping Control

From comparison of (11) and (33), it is seen that

$$\Delta\phi = k\angle\theta\Delta\delta \tag{38}$$

is satisfied, where $k \equiv \varepsilon/\varepsilon'$. We will control the firing angle according to this equation. k and θ become a gain and a phase of the control. In this subsection, we select appropriate values of these parameters.

1) Selection of Phase θ: First, we set $k = 1$. Further, we set $\Delta E = 0$ in (32) to see the effect of the control. Fig. 6 shows frequency responses of the damping torque coefficient d_e for four values of θ, where $\phi_o = 165°$. The coefficient considerably changes with θ. If we choose θ to be $\pi/2$, $-\pi/2$, or π, the damping coefficient takes negative values in some frequency ranges. However, if we choose θ to be 0, then the coefficient takes positive values at all frequencies. This means that the control is effective for all torsional modes. Thus, we select $\theta = 0$.

2) Limitation of Gain: Fig. 7(a) shows relation between the gain k and the damping torque coefficient d_e, where $\phi_o = 165°$ and $\theta = 0$. Without the control (i.e., $k = 0$), the damping torque coefficient is negative at all frequencies. Next, we increase the gain k to 1 or 2, then the damping torque coefficient moves upwards. If we increase k to 3 or 4, it comes to have positive values in some frequency range.

Fig. 7(b) shows the synchronizing torque coefficient k_e. If we increase the gain, then the coefficient decreases in a low frequency range. The synchronizing torque is closely related with the stability of the mode 6 whose frequency is 1∼2 Hz. Hence, it is not desirable that the synchronizing torque becomes negative in this frequency range. Therefore, we must set some limit on the gain.

The symbol ● in the figure shows the results obtained by numerical simulations. Phase-locked loop (PLL) is used to extract the fundamental voltage whose zero-crossing points are referred to trigger the thyristors [10]. Good agreement is seen between the simulation results and the analytical results.

3) Influence of Firing Angle: Fig. 8 shows the damping torque coefficient for cases where the firing angle is 170° or 160°. In both cases, the damping torque improves by raising the control gain. However, the required gain differs much as is clear from Figs. 7(a), 8(a), and 8(b). This means that we must adjust the gain according to the firing angle.

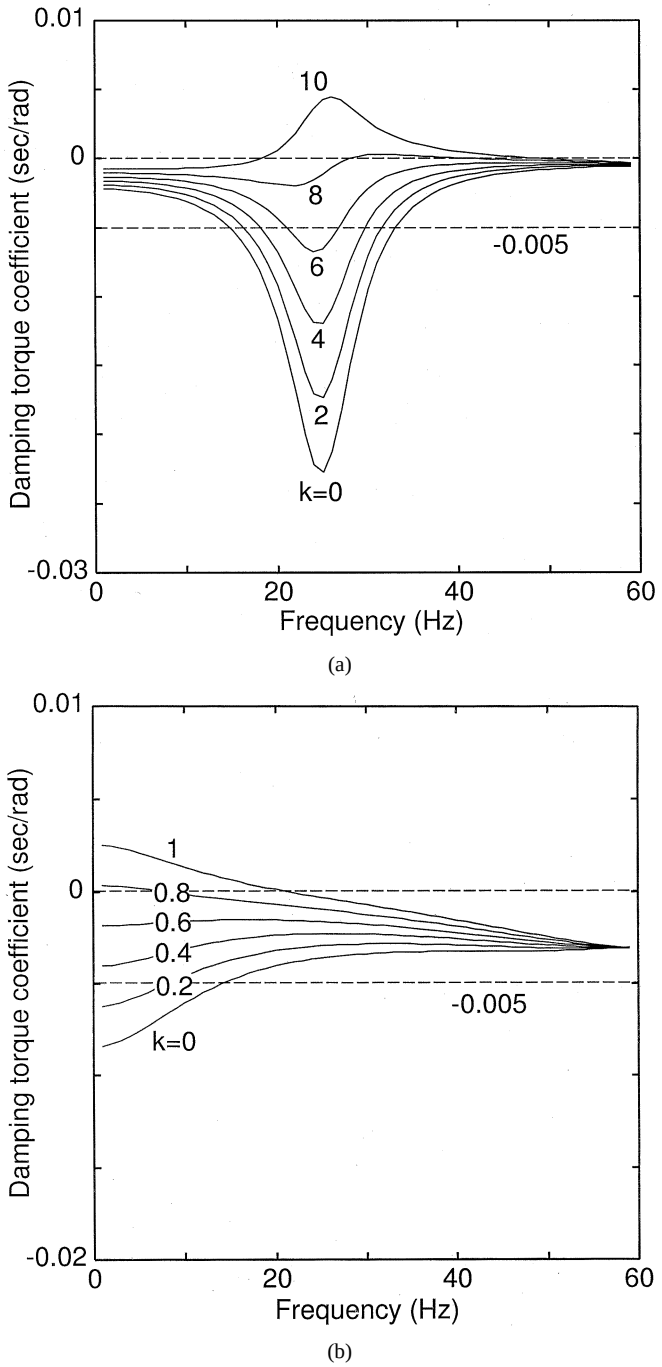

Fig. 8. Influence of firing angle. (a) Firing angle 170°. (b) Firing angle 160°.

VII. Analysis of SSR

We execute numerical simulations of SSR to verify the investigation in the preceding sections. For simplicity, we assume the mechanical damping coefficients d_1, d_2, d_3, d_4, d_6 are zero in (4)∼(9). Only d_5 is not zero. As a result, the stability of each mode is determined by the damping torque of the generator. If

$$d_e + d_5 > 0 \Rightarrow d_e > -d_5 \tag{39}$$

is satisfied at the frequency of a mode, then the mode is stable; otherwise, it is unstable. In Fig. 7(a), two lines of -0.005 and -0.002 are drawn. If the control gain k is 1.5, d_e always stays above the line of -0.005. This means that all of the modes are stable if the mechanical damping d_5 is 0.005. Similarly, if the gain is $k = 2.5$, then the modes are stable even if d_5 is 0.002.

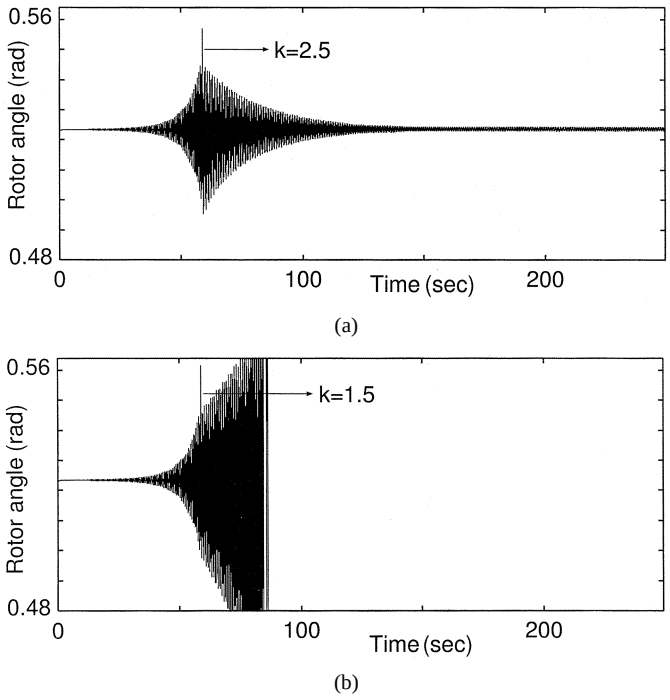

Fig. 9. Simulation of SSR ($d_5 = 0.002$). (a) $k = 0 \rightarrow 2.5$. (b) $k = 0 \rightarrow 1.5$.

TABLE III
Relation Between Control Gain k and SSR

Firing angle ϕ_o(°)	Gain k		Unstable mode
	Stable	Unstable	
170	6.5	5.5	3
165	1.5	0.5	5
160	0.4	0.2	6

Fig. 9 shows numerical simulation results. The firing angle is $\phi_o = 165°$, and the mechanical damping is 0.002. We initially set the control gain as $k = 0$, then the mode 5 of frequency 15.6 Hz grows. Next, we switch the gain at an instant. In Fig. 9(a), we switched the gain to 2.5. In this case, the oscillation of the rotor angle decays after the switching. In Fig. 9(b), we switched the gain to 1.5, however, then the mode 5 continues growing and diverges.

The mode 6 of frequency 1.2 Hz also grows in this case. Similar results are observed for the case of $d_5 = 0.005$.

Table III shows results for cases where the generator mechanical damping is $d_5 = 0.005$, and the firing angle is set at 170, 165, and 160°. In any cases, the results agree well with those predicted from Figs. 7 and 8.

From the results shown before, it is confirmed that the SSR analysis based on the analytical damping torque coefficient is valid. It is also shown that the firing angle control is effective in suppressing SSR. However, we considered a single generator on a single line as shown in Fig. 1. It is necessary to extend the

presented technique for practical systems where several generators are connected on the line. It may be useful to modify (38) as follows:

$$\Delta\phi = \sum_{i=1}^{m} k_i \angle\theta_i \Delta\delta_i \tag{40}$$

where m is the number of generators. It is not clear yet whether we can find appropriate values of the gain k_i and phase θ_i to suppress SSR of all generators. We need further investigation to show the effectiveness of (40). This remains as a future work.

VIII. Conclusions

In this paper, we made some basic consideration on the firing angle control of the thyristor-controlled series capacitor. The following conclusions apply for a single generator connected to an infinite bus by a single series compensated line.

1) If the firing angle of the thyristors oscillates at a frequency f, then the current components of frequencies $nf_o \pm f$ flow through the reactor. The analytical equations for the components were derived.

2) The current components of frequencies $nf_o \pm f$ flow through the capacitor and the transmission line. The network equation for the voltage and current components of the TCSC was derived.

3) The method of analytically calculating the damping torque of the TCSC was derived. By oscillating the firing angle in phase with the rotor angle, the damping torque is improved while some limit is imposed on the gain.

4) Lastly, the numerical simulations were executed to show that it is possible to suppress the SSR by controlling the firing angle in the proposed manner. The results agree well with the analytically predicted results.

It is thus shown that the proposed firing angle control of the TCSC is effective in suppressing SSR.

Appendix

The function in (16) is transformed as follows:

$$i_l \sin(n\omega_o + \omega)t = \sum a_i \left\{ \frac{\cos i\omega_o t_1 \sin\overline{\omega}}{i\omega_o L} + \frac{\sin(\overline{\omega} + i\omega_o)t + \sin(\overline{\omega} - i\omega_o)t}{2i\omega_o L} \right\} \tag{41}$$

where

$$\overline{\omega} = n\omega_o + \omega.$$

Substitution of (40) into (16) gives

$$i_{lsk} = \sum a_i \left\{ \frac{\cos i\omega_o t_1(\cos\overline{\omega}t_1 - \cos\overline{\omega}t_2)}{i\omega_o\overline{\omega}L} - \frac{\cos(\overline{\omega} + i\omega_o)t_1 - \cos(\overline{\omega} + i\omega_o)t_2}{2i\omega_o(\overline{\omega} + i\omega_o)L} - \frac{\cos(\overline{\omega} - i\omega_o)t_1 - \cos(\overline{\omega} - i\omega_o)t_2}{2i\omega_o(\overline{\omega} - i\omega_o)L} \right\}. \tag{42}$$

Substituting $\Delta t_1 = t_1^o + \Delta t_1, \Delta t_2 = t_2^o + \Delta t_2$ into (41), we arrange its terms as follows:

The 1st term

$$\simeq \frac{\cos i\omega_o t_1^o(\cos\overline{\omega}t_1^o - \cos\overline{\omega}t_2^o)}{i\omega_o\overline{\omega}L} - \frac{\Delta t_1 \sin i\omega_o t_1^o(\cos\overline{\omega}t_1^o - \cos\overline{\omega}t_2^o)}{\overline{\omega}L} - \frac{\cos i\omega_o t_1^o(\Delta t_1 \sin\overline{\omega}t_1^o - \Delta t_2 \sin\overline{\omega}t_2^o)}{i\omega_o L}. \tag{43}$$

The 2nd term

$$\simeq \frac{\cos(\overline{\omega} + i\omega_o)t_1^o - \cos(\overline{\omega} + i\omega_o)t_2^o}{2i\omega_o(\overline{\omega} + i\omega_o)L} - \frac{\Delta t_1 \sin(\overline{\omega} + i\omega_o)t_1^o - \Delta t_2 \sin(\overline{\omega} + i\omega_o)t_2^o}{2i\omega_o L}. \tag{44}$$

The 3rd term

$$\simeq \frac{\cos(\overline{\omega} - i\omega_o)t_1^o - \cos(\overline{\omega} - i\omega_o)t_2^o}{2i\omega_o(\overline{\omega} - i\omega_o)L} - \frac{\Delta t_1 \sin(\overline{\omega} - i\omega_o)t_1^o - \Delta t_2 \sin(\overline{\omega} - i\omega_o)t_2^o}{2i\omega_o L}. \tag{45}$$

The first terms of (43)∼(45) are steady state values, which correspond to the first term of (21). The third term of (43) cancels the second terms of (44) and (45). Lastly

The 2nd term of (43)

$$\begin{aligned} &= -\frac{2}{\overline{\omega}L}\Delta t_1 \sin i\omega_o t_1^o \sin\overline{\omega}\,\frac{t_1^o + t_2^o}{2} \sin\overline{\omega}\,\frac{t_2^o - t_1^o}{2} \\ &= \frac{2\varepsilon}{\overline{\omega}\omega_o L}\sin(hk\pi + \phi)\sin i(k\pi + \phi) \\ &\quad \times \sin(n+h)(k+1)\pi \sin(n+h)\overline{\phi} \\ &= \frac{\varepsilon \sin i\phi}{\overline{\omega}\omega_o L}\sin(n+h)\overline{\phi} \\ &\quad \times \left[\cos h\overline{\phi} - \cos h\{(2k+1)\pi + \phi\}\right] \end{aligned} \tag{46}$$

where n is even number. The term containing k of (46) is periodic, and its sum converges to zero. Thus, the second term of (21) is obtained.

Acknowledgment

The authors would like to acknowledge the suggestions of professor Tadasu Takuma in our study.

References

[1] J. Urbanek, R. J. Piwko, E. V. Larsen, B. L. Damsky, B. C. Furumasu, W. Mittlestadt, and J. D. Eden, "Thyristor controlled series compensation prototype installation at the SLATT 500kV substation," *IEEE Trans. Power Delivery*, vol. 8, pp. 1460–1469, July 1993.

[2] S. Nyati, C. A. Wegner, R. W. Delmerico, R. J. Piwko, D. H. Baker, and A. Edris, "Effectiveness of thyristor controlled series capacitor in enhancing power system dynamics: An analog simulator study," *IEEE Trans. Power Delivery*, vol. 9, pp. 1018–1027, Apr. 1994.

[3] W. Zhu, R. Spee, R. R. Mohler, G. C. Alexander, W. A. Mittelstadt, and D. Maratukulam, "An EMTP study of SSR mitigation using the thyristor controlled series capacitor," *IEEE Trans. Power Delivery*, vol. 10, pp. 1479–1485, July 1995.

[4] R. J. Piwko, C. A. Wegner, S. J. Kinney, and J. D. Eden, "Subsynchronous resonance performance tests of the Slatt thyristor-controlled series capacitor," *IEEE Trans. Power Delivery*, vol. 11, pp. 1112–1119, Apr. 1996.
[5] H. A. Othman and L. Ängquist, "Analytical modeling of thyristor-controlled series capacitors for SSR studies," *IEEE Trans. Power Syst.*, vol. 11, pp. 119–127, Feb. 1996.
[6] R. Rajaraman, I. Dobson, R. H. Lasseter, and Y. Shern, "Computing the damping of subsynchronous oscillations due to a thyristor controlled series capacitor," *IEEE Trans. Power Delivery*, vol. 11, pp. 1120–1127, Apr. 1996.
[7] B. K. Perkins and M. R. Iravani, "Dynamic modeling of a TCSC with application to SSR analysis," *IEEE Trans. Power Syst.*, vol. 12, pp. 1619–1625, Nov. 1997.
[8] P. Mattavelli, A. M. Stankovič, and G. C. Verghese, "SSR analysis with dynamic phasor model of thyristor-controlled series capacitor," *IEEE Trans. Power Syst.*, vol. 14, pp. 200–208, Feb. 1999.
[9] A. Daneshpooy and A. M. Gole, "Frequency response of the thyristor controlled series capacitor," *IEEE Trans. Power Delivery*, vol. 16, pp. 53–58, Jan. 2001.
[10] N. Kakimoto and A. Phongphanphanee, "Calculation of frequency response of thyristor-controlled series capacitor," *Trans. Inst. Elect. Eng. Jpn.*, vol. 121-B, no. 3, pp. 334–341, 2001.
[11] ——, "Calculation of damping torque of power system compensated with TCSC," *Trans. Inst. Elect. Eng. Jpn.*, vol. 121-B, no. 11, pp. 1453–1461, 2001.
[12] IEEE Committee Report, "First benchmark model for computer simulation of subsynchronous resonance," *IEEE Trans. Power Apparat. Syst.*, vol. PAS-96, pp. 1565–1570, Sept./Oct. 1977.

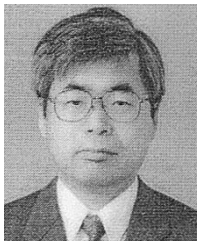

Naoto Kakimoto (M'78) was born in 1952 in Japan. He received the Ph.D. degree in electrical engineering from Kyoto University, Kyoto, Japan, in 1982.

Currently, he is an Associate Professor at Kyoto University. His current interests include power system stabilities, power electronics devices, and distributed power generations.

Dr. Kakimoto is a member of IEE of Japan.

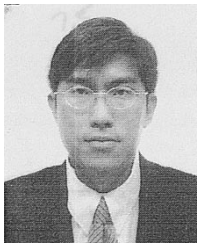

Anan Phongphanphanee was born in 1976 in Thailand. He received the M.S. degree in electrical engineering from Kyoto University, Kyoto, Japan, in 2001.

Currently, he is with the R&D department of Fujikura Ltd., Chiba, Japan.

Mr. Phongphanphanee is a member of IEE of Japan.